ABBS

Original Article

A novel multifunctional nanocomposite C225-conjugated Fe_3O_4/Ag enhances the sensitivity of nasopharyngeal carcinoma cells to radiotherapy

Di Zhao, Xinchen Sun*, Jinglong Tong, Jun Ma, Xiaodong Bu, Ruizhi Xu, and Renhua Fan

Department of Oncology, Zhongda Hospital, School of Medicine, Southeast University, Nanjing 210009, China
*Correspondence address. Tel: +86-25-83275408; Fax: +86-25-8327206; E-mail: sunxch055@yahoo.com.cn

Radiotherapy is the major treatment for nasopharyngeal carcinoma, a malignant tumor of epithelial origin. In this process, a tracer with high sensitivity is pivotal for diagnostic imaging in radiotherapy. Here, we designed a novel multifunctional magnetic silver nanocomposite, Fe_3O_4/Ag conjugated to an epidermal growth factor receptor-specific antibody (C225), which can be potentially used for synchronous cancer therapy and diagnosis via magnetic resonance imaging. Characteristics of Fe_3O_4/Ag/C225 were determined by transmission electron microscopy, energy dispersive X-ray spectroscopy, ultraviolet spectra, and dynamic light scattering. The results demonstrated that Fe_3O_4/Ag/C225 nanoparticles were spherical and dispersed well in water. The activity of C225 was preserved ∼80% in the Fe_3O_4/Ag/C225 nanoparticles. Futhermore, we tested the cytotoxicity and radiosensitivity of the nanocomposite for human nasopharyngeal carcinoma cell lines (CNEs) in vitro. MTT analysis revealed that Fe_3O_4/Ag/C225 could inhibit the proliferation of CNEs in a dose- and time-dependent manner. The clonogenic assay indicated that Fe_3O_4/Ag/C225 combined with X-ray treatment could increase the sensitivity of CNEs to irradiation. In a summary, the novel multifunctional nanocomposite Fe_3O_4/Ag/C225 might be a potential radiosensitizer for treating malign tumors in the clinic.

Keywords radiotherapy; radiosensitivity; molecular targeted therapy; nasopharyngeal carcinoma cells

Introduction

Nasopharyngeal carcinoma, a malignant tumor of epithelial origin, is one of the most common malignant tumors in southern China. Radiotherapy is the main method in the treatment of nasopharyngeal carcinoma [1,2]. However, irradiation for nasopharyngeal carcinoma has a high treatment failure rate because of its rapid growth and invasive behavior [3]. Recently, with the rapid development of imaging and computer technology, radiotherapy can now be performed in four dimensions by image guide radiation therapy (IGRT) [4]. However, as no ideal medium for trace imaging in radiotherapy is available, IGRT cannot be used to its fullest potential.

Nanomaterials have been increasingly used in biomedical fields, especially in healthcare. Nanoparticles have enormous advantages in coupling with various antibody and luminescent labeling for its characteristic of small size (≤100 nm) and surface paintability. Thus, nanoparticles can be a good tracer. Owing to the nanomaterial's physicochemical properties, nanosized particulate system can be designed specifically in collaboration with molecular biology technique, which will combine cancer diagnosis with therapy [5,6]. As we all know, the Fe_3O_4 nanoparticles are qualified for serving as magnetic resonance imaging (MRI) probes to noninvasively monitor the molecular and cellular event in vivo. Fe_3O_4 nanoparticles also can couple together with proteins like some antibodies, which will induce the biological therapeutic effects [7,8]. By this means, diagnosis and treatment could be implemented synchronously.

Epidermal growth factor receptor (EGFR) is a tyrosine kinase receptor, which is important in the phosphatidylinositol 3-kinase (PI3K)/Akt signaling pathway [9]. The overexpression of EGFR correlates to cell proliferation, angiogenesis, and tumor growth, and may induce tumor cells to metastasize [10,11]. Clinical studies have shown that the patients with brain metastasis have the overexpression of human EGFR2 and/or EGFR [12,13]. EGFR inhibitors have been used to treat the advanced cancer patients by interrupting the PI3K/Akt-signaling cascades [14]. Several different EGFR antibodies including humanized monoclonal antibodies such as cetuximab (Erbitux, Merck Serono Ltd., Darmstadt, Germany) have been used to treat the head and neck tumor associated with radiotherapy, which can improve locoregional control and reduce mortality without increasing common toxic effects [15].

In this study, we reported a novel multifunctional magnetic−particle−silver nanocomposite system. In this system, the core of the composite Fe_3O_4/Ag/C225 particle, Fe_3O_4, can

be used as a tumor tracer for radiation therapy, and silver has been previously described as a radiation sensitizer [16]. The EGFR-specific antibody (C225) has been successfully used as an anti-tumor treatment in clinical studies [15]. Then this magnetic silver nanocomposite could be potentially used for targeted cancer detection by MRI as well as for synchronous cancer therapy via a therapeutic antibody with pro-apoptotic effects. Furthermore, we found the composite particle Fe$_3$O$_4$/Ag/C225-inhibited CNEs proliferation and increased the sensitivity to irradiation. Therefore, Fe$_3$O$_4$/Ag/C225 might be a potential radiosensitizer for treating malign tumors in the clinic.

Materials and Methods

Chemicals and reagents

All chemicals used in this experiment were of analytical reagent grade. Ferrous sulfate (FeSO$_4$•7H$_2$O), oleic acid, dimethyl sulfoxide (DMSO), n-hexane, acetone, acetic acid, anhydrous sodium acetate, absolute alcohol, and 2,3-dimercaptosuccinic acid (DMSA) were purchased from Sinopharm Chemical Reagent Co. Ltd (Shanghai, China). Sodium borate and boric acid were reagents from Shanghai Lingfeng Chemical Reagent Co. Ltd (Shanghai, China). Tetramethylammonium hydroxide was supplied by Shanghai Zhuorui Chemical Reagent Co. Ltd (Shanghai, China). 1-Ethyl-3-(3-dimethyllaminopropyl) carbodiimide hydrochloride (EDC) and 1-hydroxy-2,5-pyrrolidinedione (NHS) were purchased from Sigma Aldrich (St Louis, USA). Albumin bovine (BSA) was obtained from the Nanjing Bookman Biotechnology Ltd (Nanjing, China). Nimotuzu monoclonal antibody was from Beijing BaiTai Biopharmaceutical Co. Ltd (Beijing, china). Hydrodynamic size distributions of Fe$_3$O$_4$/Ag were assessed by dynamic light scattering (Beckman, Pasadena, USA). C225 (cetuximab) was purchased from Merck Serono (Darmstadt, Germany).

Preparation of DMSA-modified Fe$_3$O$_4$ nanoparticles and Fe$_3$O$_4$/Ag/C225 nanocomposites

Oleate-capped Fe$_3$O$_4$ nanoparticles were prepared. FeSO$_4$•7H$_2$O (3 mmol), oleic acid (10 ml), N(CH$_3$)$_4$OH (10 ml), and DMSO (35 ml) were mixed in a 100-ml three-necked bottle, and the mixture was refluxed at 140°C for 1 h with stirring in the presence of N$_2$. A black precipitate was obtained by magnetic separation and washed with alcohol three times. The obtained oleate-capped Fe$_3$O$_4$ nanoparticles were dried overnight in a vacuum. In order to conjugate to the antibody, surface functionalization was carried out by ligand exchange reaction. In brief, carboxylated Fe$_3$O$_4$ nanoparticles, Fe$_3$O$_4$/DMSA, were prepared by stirring a mixture of oleate-capped Fe$_3$O$_4$ nanoparticles and DMSA (mass ratio of 1 : 1) in acetone (9 ml) at 60°C for

4 h. The black precipitate was obtained via magnetic separation, washed with alcohol three times and dispersed in water. Fe$_3$O$_4$/Ag nanoparticles were synthesized by the reverse micelle method. One hundred microliters of 40 mM Fe$_3$O$_4$ nanoparticles were mixed with a W/O microemulsion containing 1.4 ml of Triton X-100, 1.4 ml of n-hexanol, and 7.5 ml of cyclohexane, with vigorous stirring. Then, 200 µl of 0.1 M AgNO$_3$ was added. After 30 min, 200 µl of 0.2 M NaBH$_4$ was added to the solution. The mixture was stirred at room temperature for 4 h. The black Fe$_3$O$_4$/Ag nanoparticles were precipitated by adding excess acetone, and then centrifuged and repeatedly washed with ethanol and water to remove surfactant and unreacted materials. The obtained nanoparticles were suspended in water for future use. Conjugation of C225 to the Fe$_3$O$_4$/Ag by adding borax buffer (PH 9.0) to adjust pH value to 7.9, blocking the reaction by adding 4% BSA solution (400 µl) with continuous shaking at 37°C for 1 h, then adding C225 to Fe$_3$O$_4$/Ag with continuous shaking at 37°C for 30 min. Finally, Fe$_3$O$_4$/Ag/C225 nanoparticles were obtained by adding certain amount of purified water to resuspend nanoparticles after centrifugation at 11,742 g at 4°C for 1 h. The conjugated nanoparticles were purified by gel chromatography (GE sephacryl s-300, Pittsburgh, USA). The final Fe$_3$O$_4$/Ag/C225 composites were stored at 4°C. The particle size and morphology of the Fe$_3$O$_4$/Ag/C225 composites were characterized by transmission electronic microscopy (TEM; JEOL JEM-2100, Tokyo, Japan). Photon correlation spectroscopy was used to determine the hydrodynamic size distribution using a Beckman Coulter N4 Plus Submicron Particle Analyzer.

Cell culture

CNE cells were purchased from the the Cell Bank of the Chinese Academy of Sciences (Shanghai, China). Cells were cultured in a humidified atmosphere containing 5% CO$_2$ in RPMI 1640 medium (Gibco, Carlsbad, USA) supplemented with heat-inactivated fetal bovine serum (15% by volume), penicillin G (50 U/ml), and streptomycin (50 µg/ml). The cell line was maintained in the exponential growth phase and provided with fresh medium every 2−3 days.

Enzyme-linked immunosorbent assay

We used a double antibody sandwich enzyme-linked immunosorbent assay (ELISA) to test the level of C225 in the nanocomposite, Fe$_3$O$_4$/Ag/C225. CNEs were seeded in a 96-well plate in 300-µl medium at a density of 0.8 × 10^4 cells/well and then cultured for 2 days. Then the cells were washed with phosphate buffered saline (PBS) four times, and fixed with pre-cooled 0.125% pentyl glycol for 30 min at 4°C. After that the cells were incubated in 1% BSA at 37°C for 1 h to block non-specific binding, and

then washed twice. The serially diluted C225 and different concentrations of Fe$_3$O$_4$/Ag/C225 were added to the 96-well plate. Horseradish peroxidase (HRP)-conjugated anti-mouse immunoglobulin G (IgG) (1 : 2000, Zhongshan Goldbride Ltd., Beijing, China) was added, followed by the TMB (Horseradish Peroxidase Color Development Solution). Positive and negative control wells were included to quantify protein levels for all samples. The absorbance was measured at 450 nm using a microplate spectrophotometer (SpectraMax Molecular Devices, Sunnyvale, USA).

3-(4,5-Dimethylthiazol-2-yl)-2,5-diphenyltetrazolium bromide assay

To measure the cytotoxicity of Fe$_3$O$_4$/Ag/C225, cells were seeded in 96-well plates at a density of 2.5×10^4 cells/well and allowed to adhere for 24 h at 37°C. The cells were cultured in the presence of different concentration of Fe$_3$O$_4$/Ag/C225 (0, 50, 100, 200, 400, and 800 µg/L) for 24–48 h, followed by 3-(4,5-Dimethylthiazol-2-yl)-2,5-diphenyltetrazolium bromide (MTT) (Sigma) treatment for 4 h at 37°C. Then DMSO was added to each well to dissolve the dark blue crystal product. The absorbance was measured at 488 nm using a microplate reader (Bio-Rad, Hercules, USA).

Clonogenic assay

Exponentially growing cells were irradiated at the doses of 0, 1, 2, 4, 6, and 8 Gy at room temperature, followed by being treated with or without Fe$_3$O$_4$/Ag/C225 treatment for 24 h. Then the cells were seeded in a 24-well plate at a density of 200 cells/well, and cultured for 10–14 days. Plates were washed in PBS and the colonies were fixed with 95% ethanol. Staining was carried out with 0.1% crystal violet solution. Colonies of >50 cells were counted to calculate the surviving fraction. Six parallel samples were scored for each treatment condition.

Western blot analysis

Treated and untreated cells were lysed in extraction buffer [1% sodium dodecyl sulfate (SDS), 1 mM Na$_3$VO$_4$, 0.1 M Tris (pH 7.4)], plus protease inhibitor mixture (Roche, Indianapolis, USA), and phosphatase inhibitor mixture (Upstate Biotechnology, Lake Placid, USA) at 4°C. The protein concentration was measured using a protein assay kit according to the manufacturer's instructions (Bio-Rad). Proteins (40 µg/lane) were running on a 5% or 10% SDS-polyacrylamide gel, and then transferred to polyvinylidene difluoride membranes (Millipore, Bedford, USA). The membranes were blocked with 5% non-fat dried milk for 4 h in PBS—0.1% Tween (PBST) and probed with C225 (1 : 1000) at 4°C overnight. After three times washing with PBST, the membranes were incubated with

HRP-conjugated goat anti-rabbit IgG (1 : 100) (Promega, Madison, USA) for 2 h, and were visualized using ECL chemiluminescent substrate (GE Healthcare Life Sciences, Fairfield, USA).

Statistical analysis

Data were expressed as the mean $\pm$ standard error (SE). SPSS version 16 (SPSS, Chicago, USA) was used to analyze one-way analysis of variance followed by a Student–Newman–Keuls test. $P < 0.05$ was considered statistical significant.
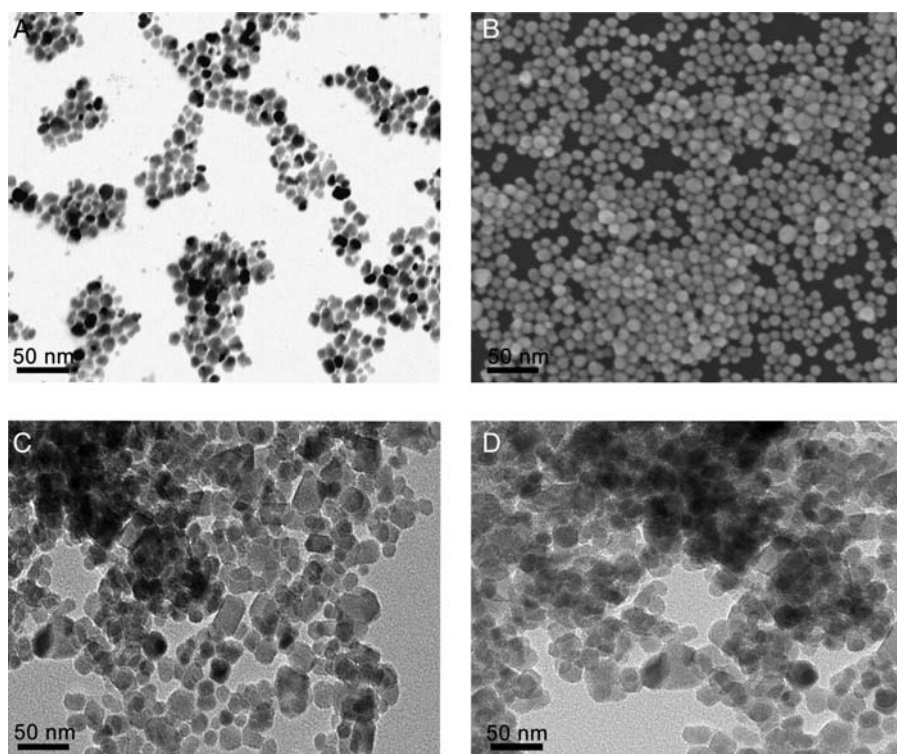
Results

The characteristics of Fe$_3$O$_4$/Ag/ C225 nanocomposites

Figure 1(A–D) shows the morphology of Fe$_3$O$_4$, AgNPs, Fe$_3$O$_4$/Ag and Fe$_3$O$_4$/Ag/C225 nanoparticles determined by TEM. The majority of magnetic nanoparticles were spherical or nearly spherical. The Fe$_3$O$_4$/Ag/C225 particle sizes were small in a range between 25 and 35 nm, which is larger than that of Fe$_3$O$_4$ and Ag. And there is no significant difference in size compared with Fe$_3$O$_4$/Ag under TEM.

To confirm the composition of the composites, EDS spectrum *in situ* composition analysis was collected. The result showed the presence of silver, iron, and oxygen in the composites [Fig. 2(A)]. The diffraction peaks of silver, iron, and oxygen exist in the pattern, which indicated that Fe$_3$O$_4$/Ag nanocomposites have been successfully synthesized. The ultraviolet spectra of the nanocomposite indicated that the absorption peak of Fe$_3$O$_4$/Ag at 423 nm gradually increased after binding to Fe$_3$O$_4$, with a red shift from 390 to 423 nm [Fig. 2(B)]. The hydrodynamic size distributions of Fe$_3$O$_4$/Ag and Fe$_3$O$_4$/Ag/C225 as assessed by dynamic light scattering were 35.98 ± 15.15 nm and 102.34 ± 42.12 nm, respectively [Fig. 2(C)]. The larger hydrodynamic size of magnetic nanoparticles was attributed to the presence of the antibody C225 in the hydration layer and the particle aggregations in water. The results of *in vitro* release rate testing revealed that the nanocomposites were released slowly and steadily [Fig. 2(D)].

### The activity of the EGFR antibody is preserved in Fe$_3$O$_4$/Ag/C225 nanoparticles

The results of ELISA showed that the activity of the EGFR antibody in the nanocomposites Fe$_3$O$_4$/Ag/C225 was preserved ~80%. Furthermore, when the concentration decreased the preserved activity increased. When the concentration of the pure C225 antibody was 500 µg/L, the activity of the C225 in the Fe$_3$O$_4$/Ag/C225 was $76.82\% \pm 2.12\%$. However, when the concentration of C225 was 72.5 µg/L, the preserved activity was $83.17\% \pm 3.23\%$.

Figure 1 TEM of Fe$_3$O$_4$/Ag/C225 nanoparticles (A) The morphology of Fe$_3$O$_4$ nanoparticles. (B) The morphology of AgNPs. (C) The morphology of Fe$_3$O$_4$/Ag nanoparticles. (D) The morphology of Fe$_3$O$_4$/Ag/C225 nanoparticles.
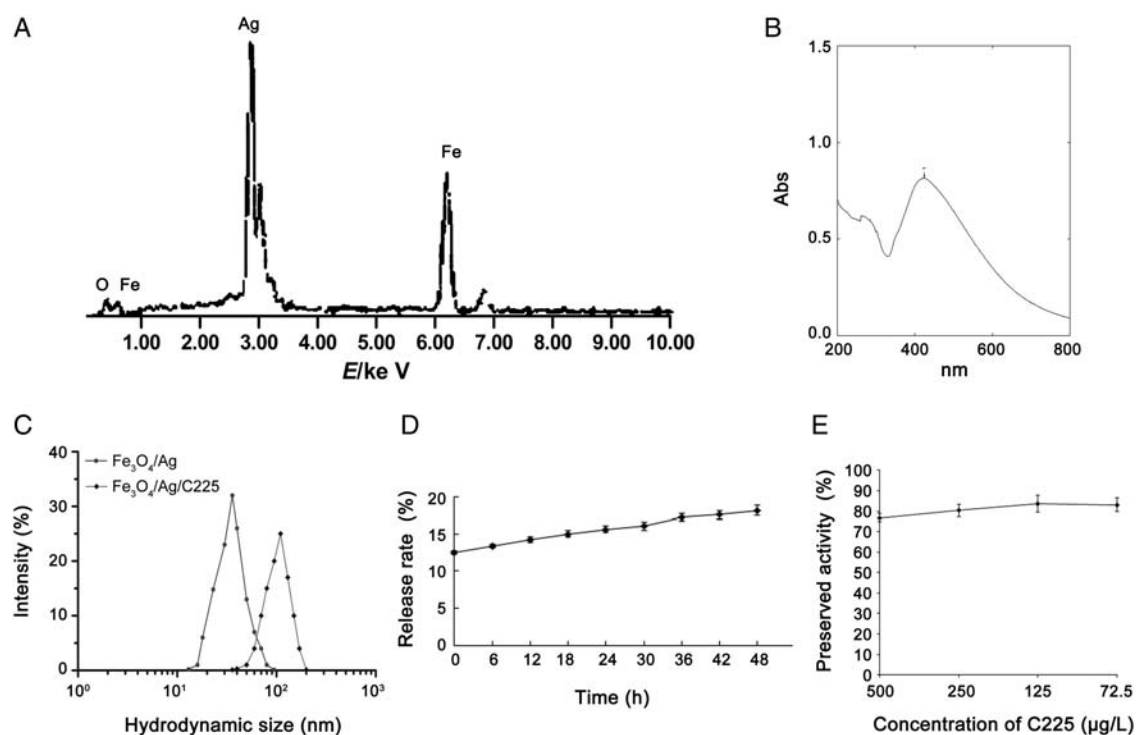
Figure 2 Characteristics of Fe$_3$O$_4$/Ag/C225 nanoparticles (A) EDS spectrum of Fe$_3$O$_4$/Ag composites. (B) The absorption peak of Fe$_3$O$_4$/Ag at 423 nm. (C) Hydrodynamic size distributions of Fe$_3$O$_4$/Ag and Fe$_3$O$_4$/Ag/C225 nanoparticles were assessed by dynamic light scattering. (D) The release rate of Fe$_3$O$_4$/Ag/C225 under *in vitro* conditions. (E) The activity preservation of C225 in the nanocomposite Fe$_3$O$_4$/Ag/C225 was analyzed by ELISA.
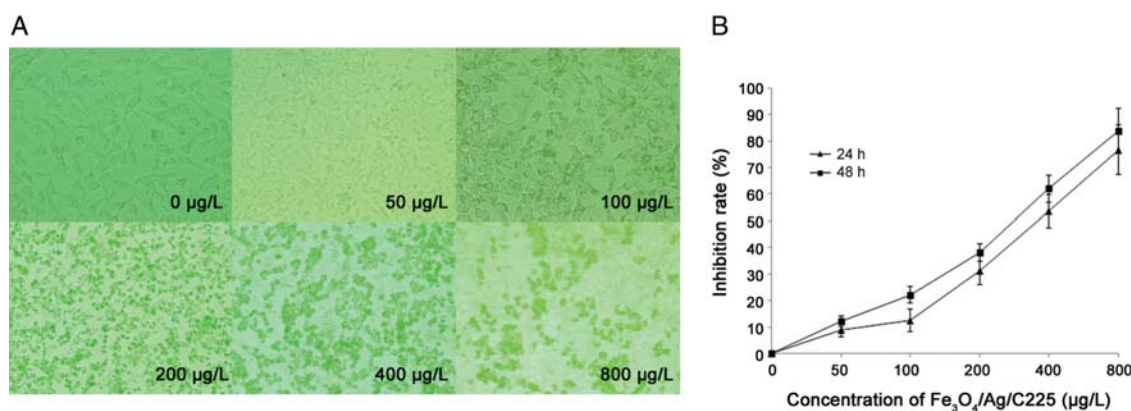
Figure 3 Effect of Fe$_3$O$_4$/Ag/C225 on CNE cells proliferation (A) The morphology of CNE cells under the different concentration of Fe$_3$O$_4$/Ag/C225 treatment ($\times$200). (B) MTT assays showed that Fe$_3$O$_4$/Ag/C225 inhibited cell growth in a concentration-dependent manner.

Thus, C225 activity in the Fe$_3$O$_4$/Ag/C225 nanocomposite was well preserved [**Fig. 2(E)**].

Fe$_3$O$_4$/Ag/C225 inhibits the proliferation of CNE cells

When CNEs were treated with Fe$_3$O$_4$/Ag/C225 at different concentrations (0, 50, 100, 200, 400, 800 μg/L) for 24 h, the morphology of the cells changed from polygonal to round, and the cell numbers also decreased [**Fig. 3(A)**]. MTT assays showed that Fe$_3$O$_4$/Ag/C225 inhibited cell growth in a concentration-dependent manner with an IC$_{50}$ of 350.49 $\pm$ 3.14 μg/L and 262.53 $\pm$ 4.47 μg/L for 24 and 48 h exposure, respectively ($P <$ 0.05) [**Fig. 3(B)**].

Fe$_3$O$_4$/Ag/C225 enhances the sensitivity of CNE cells to X-ray irradiation

The effects of Fe$_3$O$_4$/Ag/C225 on the cytotoxicity of X-ray irradiation in CNE cells were investigated using clonogenic assay (**Fig. 4**). Cells were first irradiated at different doses of X-rays (0, 1, 2, 4, 6, and 8 Gy), then incubated with 50 μg/L Fe$_3$O$_4$/Ag and 30 μg/L Fe$_3$O$_4$/Ag/C225 ($\sim$1/9 concentration of IC$_{50}$) for 24 h. This concentration of Fe$_3$O$_4$/Ag and Fe$_3$O$_4$/Ag/C225 and exposure time were not cytotoxic (data not shown). Cell survival curves were plotted with a single-hit multitarget model to yield values of the relative parameters. The parameter D0 was used to characterize the radiosensitivity in the linear (high dose) region, and the value of parameter Dq indicated the cells ability to repair potentially lethal damage in the shoulder (low dose) region. According to the **Fig. 4**, for X-ray irradiated CNE cells without Fe$_3$O$_4$/Ag and Fe$_3$O$_4$/Ag/C225 treatment, the D0 and Dq values were 2.852 $\pm$ 0.074 and 2.124 $\pm$ 0.121 Gy, respectively. For the cells synchronously treated under irradiation and Fe$_3$O$_4$/Ag or Fe$_3$O$_4$/Ag/C225, the D0 values were 1.923 $\pm$ 0.012 Gy (for Fe$_3$O$_4$/Ag) and 1.261 $\pm$ 0.023 Gy (for Fe$_3$O$_4$/Ag /C225), and the Dq values were 1.792 $\pm$ 0.004 (for Fe$_3$O$_4$/Ag) and 1.704 $\pm$ 0.032 Gy (for Fe$_3$O$_4$/Ag /C225), respectively. Therefore,
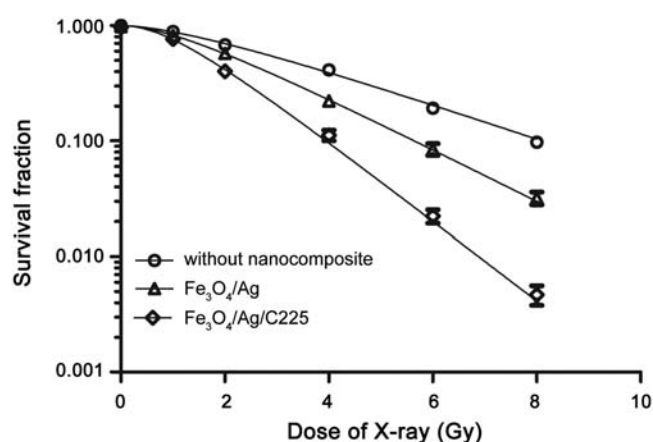

Figure 4 Fe$_3$O$_4$/Ag/C225 enhances the radiosensitivity of CNE cells Exponentially growing CNE cells were plated 24 h prior to irradiation. After irradiation, incubated with 50 μg/L Fe$_3$O$_4$/Ag and 30 μg/L Fe$_3$O$_4$/Ag/C225 for 24 h. Colony-forming efficiency was determined 10–14 days later, and the survival fractions of Fe$_3$O$_4$/Ag- or Fe$_3$O$_4$/Ag/C225-treated cells were calculated by normalizing to the colony-forming efficiency of untreated cells.

Fe$_3$O$_4$/Ag/C225 potentiates the cytotoxicity of X-rays in CNE cells compared with Fe$_3$O$_4$/Ag alone $\sim$1.525 fold (D0 for Fe$_3$O$_4$/Ag compared with D0 for Fe$_3$O$_4$/Ag/C225). The effect was observed at 30 μg/L Fe$_3$O$_4$/Ag/C225 ($P <$ 0.05). In addition, Fe$_3$O$_4$/Ag/C225 enhanced the cytotoxicity of X-rays in CNE cells by $\sim$2.262 fold compare with X-rays alone (D0 for without Fe$_3$O$_4$/Ag and Fe$_3$O$_4$/Ag/C225 treatment compare with D0 for Fe$_3$O$_4$/Ag/C225).

Fe$_3$O$_4$/Ag/C225 down-regulates the expression of EGFR

To explore the molecular mechanism of Fe$_3$O$_4$/Ag/C225-sensitizing CNE cells to irradiation, we further detected the expression of EGFR in CNE cell lines when treated with Fe$_3$O$_4$/Ag/C225 combined with X-ray irradiation. Western blot analysis showed that Fe$_3$O$_4$/Ag/C225 or irradiation alone decreased the expression levels of EGFR,
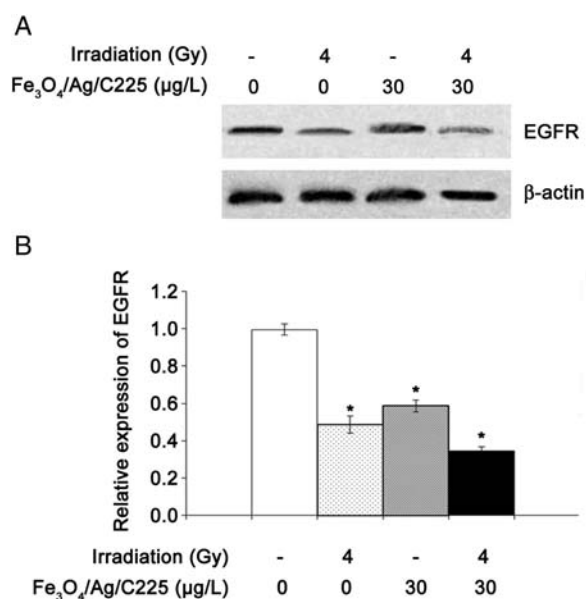
Figure 5 Fe$_3$O$_4$/Ag/C225 combined with X-ray inhibits the expression of EGFR in CNE cells (A) CNEs treated with Fe$_3$O$_4$/Ag/C225 and X-ray irradiation had reduced EGFR protein levels compared with controls (without irradiation and Fe$_3$O$_4$/Ag/C225 treatment). (B) Quantification of the western blot results from three times independent experiments. *$P < 0.05$ compared with untreated CNEs.

whereas Fe$_3$O$_4$/Ag/C225 inhibited the expression of EGFR more dramatically when combined with irradiation (**Fig. 5**), which indicates that Fe$_3$O$_4$/Ag/C225 treatment might increase the radiosensitivity of CNE cells by inhibiting the expression of EGFR.

Discussion

Radiation therapy is one of the main treatments for malignant tumors, and ~70% of cancer patients require radiation therapy [17]. IGRT is used to accurately target tumors, especially in head and neck malignant tumors. Meanwhile, IGRT allows to optimize the dose of irradiation according to the target tumor volume [18]. Therefore, IGRT can reduce the radiation dose on the surrounding normal tissue considering the three-dimensional shape and density of the tumor. An imaging tracer with high sensitivity, specificity, and safety is important for acquiring the high-resolution imaging. However, currently it is hard to find an ideal tracer in the clinical imaging. Although radionuclide imaging methods can evaluate the function of transplanted cells, the sensitivity and spatial resolution are low, and the safety also is an issue [19–21]. In addition, fluorescence-imaging technology can provide images with low background noise and high sensitivity, but so far they only have been used in animal studies. Furthermore, the spatial resolution is poor, anatomical details are not apparent, and the fluorescent light only can image a shallow depth, which will limit its clinical application [22–24].

In this study, we synthesized a new multi-functional composite nanoparticle, Fe$_3$O$_4$/Ag/C225, which could be potentially used for cancer therapy and diagnosis at the same time. The Fe$_3$O$_4$/Ag/C225 formulation, using super-paramagnetic Fe$_3$O$_4$ nanoparticles, had good characteristics for MRI [25,26]. Aggregates of magnetic nanoparticles can produce magnetic kernels to enhance the sensitivity of MRI. Thus, the use of Fe$_3$O$_4$ nanoparticles as MRI agent might provide new and highly effective imaging tracers for *in vivo* tumor cell radiotherapy. Our previous studies have demonstrated that AgNPs could enhance the inhibitory effect of radiation on tumor cells, and could be used as radiosensitizers for improving the efficiency of radiotherapy [16]. C225 is the specific monoclonal antibody of EGFR and has been used in clinics to inhibit tumor cell growth. C255 also has been proved to be a radiation-sensitizer. As EGFR is highly expressed in most solid tumors and the antibody possesses a high affinity for its antigen, C225 in the Fe$_3$O$_4$/Ag/C225 formulation might play an important role as an imaging tracer *in vivo* and *in vitro* by binding to the EGFR.

We first conjugated Fe$_3$O$_4$ core with AgNPs by EDC/NHS coupling chemistry, followed by coupling C225 by surface chemical bonds. Then we confirmed the successful synthesis of the nanocomposite by TEM, EDS, ultraviolet spectra, and dynamic light scattering (**Fig. 2**). The curve of nanocomposite release showed that the Fe$_3$O$_4$/Ag/C225 was stable *in vitro*. As nanocomposites are important for biological applications, we tested the activity preservation of the antibody by ELISA. The results showed that the activity preservation of C225 in the Fe$_3$O$_4$/Ag/C225 nanocomposites was increased when the concentration of C225 decreased. Furthermore, we explored the effect of Fe$_3$O$_4$/Ag/C225 on CNE cells *in vitro*. MTT assay indicated that Fe$_3$O$_4$/Ag/C225 had an inhibitory effect on CNE cells in a dose-dependent manner (**Fig. 3**). Meanwhile, Fe$_3$O$_4$/Ag/C225 and X-ray treatment could synergistically improve the efficiency of radiotherapy (**Fig. 4**). Fe$_3$O$_4$/Ag/C225 treatment enhanced the cytotoxicity of X-rays in CNE cells ~2.262 fold, which indicated that Fe$_3$O$_4$/Ag/C225 might be a useful radiosensitizer for improving the outcome of cancer radiotherapy.

EGFR play an important role in cancer development and progression, especially in a variety of human malignancies including lung, head and neck, colon, breast, ovary, and glioma cancer [27]. The majority of head and neck cancers is squamous cell carcinomas, and commonly over-expresses EGFR [28]. In addition, the high expression or activation of EGFR correlates with the radioresistance of cells and tumors [29–31]. In order to investigate the mechanisms of Fe$_3$O$_4$/Ag/C225-induced inhibition in CNEs when combined with X-rays, we measured the expression of EGFR proteins. Western blot results showed

that Fe$_3$O$_4$/Ag/C225 combined with X-ray irradiation treatment remarkably inhibited the expression level of EGFR compared with X-ray treatment alone (**Fig. 5**). Thus, Fe$_3$O$_4$/Ag/C225 might enhance the sensitivity of CNEs to irradiation by inhibiting EGFR expression.

In conclusion, we synthesized a multi-functional Fe$_3$O$_4$/Ag/C225 nanocomposite, which may be used as a potent radiosensitizer and imaging tracers for treating malign tumors in radiotherpy. In the future, *in vivo* MRI will be performed in order to further explore the sensitivity of Fe$_3$O$_4$/Ag/C225 composites as a tracer *in vivo*. And the effect of Fe$_3$O$_4$/Ag/C225 composites on the radiotherapy *in vivo* also will be confirmed. The novel multifunctional nanocomposite Fe$_3$O$_4$/Ag/C225 might be a potential radiosensitizer for treating malign tumors in the clinic. Fe$_3$O$_4$/Ag also can be coupled with other antibodies, which will provide a wide application in cancer therapy.

Funding

References

1 Rottey S, Madani I, Deron P and Van Belle S. Modern treatment for nasopharyngeal carcinoma: current status and prospects. Curr Opin Oncol 2011, 23: 254–258.

2 Lapeyre M, Belliere A, Hoffstetter S and Peiffert D. Brachytherapy for head and neck cancers (nasopharynx excluded). Cancer Radiother 2008, 12: 515–521.

3 Chan AT. Nasopharyngeal carcinoma. Ann Oncol 2010, 21(Suppl. 7): i308–i312.

4 Tang G, Earl MA, Luan S, Wang C, Mohiuddin MM and Yu CX. Comparing radiation treatments using intensity-modulated beams, multiple arcs, and single arcs. Int J Radiat Oncol Biol Phys 2010, 76: 1554–1562.

5 Chung YC, Chen IH and Chen CJ. The surface modification of silver nanoparticles by phosphoryl disulfides for improved biocompatibility and intracellular uptake. Biomaterials 2008, 29: 1807–1816.

6 Verma A, Uzun O, Hu Y, Hu Y, Han HS, Watson N and Chen S, *et al*. Surface-structure-regulated cell-membrane penetration by monolayer-protected nanoparticles. Nat Mater 2008, 7: 588–595.

7 Cedervall T, Lynch I, Lindman S, Berggard T, Thulin E, Nilsson H and Dawson KA, *et al*. Understanding the nanoparticle-protein corona using methods to quantify exchange rates and affinities of proteins for nanoparticles. Proc Natl Acad Sci U S A 2007, 104: 2050–2055.

8 Lundqvist M, Stigler J, Elia G, Lynch I, Cedervall T and Dawson KA. Nanoparticle size and surface properties determine the protein corona with possible implications for biological impacts. Proc Natl Acad Sci U S A 2008, 105: 14265–14270.

9 Naumann RW. The role of the phosphatidylinositol 3-kinase (PI3K) pathway in the development and treatment of uterine cancer. Gynecol Oncol 2011, 123: 411–420.

10 Herchenhorn D and Ferreira CG. Targeting epidermal growth factor receptor to optimize chemoradiotherapy in locally advanced head and neck cancer: has biology been taken into account? J Clin Oncol 2011, 29: e283–e284, e285–e287.

11 Lurje G and Lenz HJ. EGFR signaling and drug discovery. Oncology-Basel 2009, 77: 400–410.

12 Hicks DG, Short SM, Prescott NL, Tarr SM, Coleman KA, Yoder BJ and Crowe JP, *et al*. Breast cancers with brain metastases are more likely to be estrogen receptor negative, express the basal cytokeratin CK5/6, and over-express HER2 or EGFR. Am J Surg Pathol 2006, 30: 1097–1104.

13 Perez EA and Spano JP. Current and emerging targeted therapies for metastatic breast cancer. Cancer 2012, 118: 3014–3025.

14 Gril B, Palmieri D, Bronder JL, Herring JM, Vega-Valle E, Feigenbaum L and Liewehr DJ, *et al*. Effect of lapatinib on the outgrowth of metastatic breast cancer cells to the brain. J Natl Cancer Inst 2008, 100: 1092–1103.

15 Bonner JA, Harari PM, Giralt J, Azarnia N, Shin DM, Cohen RB and Jones CU, *et al*. Radiotherapy plus cetuximab for squamous-cell carcinoma of the head and neck. N Engl J Med 2006, 354: 567–578.

16 Liu L, Ni F, Zhang J, Jiang X, Lu X, Guo Z and Xu R. Silver nanocrystals sensitize magnetic-nanoparticle-mediated thermo-induced killing of cancer cells. Acta Biochim Biophys Sin 2011, 43: 316–323.

17 Pajonk F, Vlashi E and McBride WH. Radiation resistance of cancer stem cells: the 4 R's of radiobiology revisited. Stem Cells 2010, 28: 639–648.

18 Kainz K, Chen GP, Chang YW, Prah D, Sharon QX, Shukla HP and Stahl J, *et al*. A planning and delivery study of a rotational IMRT technique with burst delivery. Med Phys 2011, 38: 5104–5118.

19 Hoffman JM and Gambhir SS. Molecular imaging: the vision and opportunity for radiology in the future. Radiology 2007, 244: 39–47.

20 Hauger O, Frost EE, van Heeswijk R, Deminiere C, Xue R, Delmas Y and Combe C, *et al*. MR evaluation of the glomerular homing of magnetically labeled mesenchymal stem cells in a rat model of nephropathy. Radiology 2006, 238: 200–210.

21 Barnett BP, Arepally A, Karmarkar PV, Qian D, Gilson WD, Walczak P and Howland V, *et al*. Magnetic resonance-guided, real-time targeted delivery and imaging of magnetocapsules immunoprotecting pancreatic islet cells. Nat Med 2007, 13: 986–991.

22 Tai JH, Foster P, Rosales A, Feng B, Hasilo C, Martinez V and Ramadan S, *et al*. Imaging islets labeled with magnetic nanoparticles at 1.5 Tesla. Diabetes 2006, 55: 2931–2938.

23 Politi LS. MR-based imaging of neural stem cells. Neuroradiology 2007, 49: 523–534.

24 Dave SR and Gao X. Monodisperse magnetic nanoparticles for biodetection, imaging, and drug delivery: a versatile and evolving technology. Wiley Interdiscip Rev Nanomed Nanobiotechnol 2009, 1: 583–609.

25 Fujita H. New horizons in MR technology: RF coil designs and trends. Magn Reson Med Sci 2007, 6: 29–42.

26 Laurent S, Boutry S, Mahieu I, Vander EL and Muller RN. Iron oxide based MR contrast agents: from chemistry to cell labeling. Curr Med Chem 2009, 16: 4712–4727.

27 Bronte G, Terrasi M, Rizzo S, Sivestris N, Ficorella C, Cajozzo M and Di Gaudio F, *et al*. EGFR genomic alterations in cancer: prognostic and predictive values. Front Biosci (Elite Ed) 2011, 3: 879–887.

28 Specenier P and Vermorken JB. Cetuximab in the treatment of squamous cell carcinoma of the head and neck. Expert Rev Anticancer Ther 2011, 11: 511–524.

29 Nyati MK, Morgan MA, Feng FY and Lawrence TS. Integration of EGFR inhibitors with radiochemotherapy. Nat Rev Cancer 2006, 6: 876–885.

30 Larsen AK, Ouaret D, El OK and Petitprez A. Targeting EGFR and VEGF(R) pathway cross-talk in tumor survival and angiogenesis. Pharmacol Ther 2011, 131: 80–90.

31 Hatanpaa KJ, Burma S, Zhao D and Habib AA. Epidermal growth factor receptor in glioma: signal transduction, neuropathology, imaging, and radioresistance. Neoplasia 2010, 12: 675–684.